



# Validation of a High-Throughput Wound Healing Assay using 3D Cell Patterning and Automated, Kinetic Imaging

Brad Larson<sup>1</sup>, Glauco R. Souza<sup>2</sup>, William Haisler<sup>2</sup>, Jan Seldin<sup>3</sup>, and Peter Banks<sup>1</sup>

<sup>1</sup>BioTek Instruments, Inc. | Winooski, VT | USA • <sup>2</sup>Nano3D Biosciences, Inc. | Houston, TX | USA • <sup>3</sup>Greiner Bio-One, Inc. | Monroe, NC | USA



## Abstract

Wound healing, both acute and chronic, involves a complex internal and external choreography of signaling, in addition to interactions with neighboring cells and the surrounding environment or external stimuli, and cell migration. This synergistic relationship can also vary depending on the wound type. Therefore, characterizing the mechanisms therein is of great interest for many applications, including wound dressing, burn and ulcer healing, scar elimination, anti-aging and aesthetic cosmetics and much more. Historically, most wound healing assays use a scratch technique, where a confluent two-dimensional (2D) cell layer is mechanically injured, and cell migration is measured. Major limitations of this method are the lack of biomimetic environment, *in vivo*-like architecture and multi-cellular network, and as scratching methods vary, results are difficult to replicate. Newer three-dimensional (3D) methods allow cells to self-aggregate in the absence of a solid substrate. Vital cell-cell and cell-extracellular matrix (ECM) communication networks are able to be reestablished. In this way, both cellular morphology and behavior more closely mimic that found in the body.

Here, we demonstrate a novel 3D wound healing assay model that can overcome 2D assay limitations. The method incorporates magnetic levitation where cells are first incubated with a nontoxic, magnetic nanoparticle assembly which does not induce an inflammatory cytokine response. The cells are then placed into a microplate well and levitated by placing a magnet above the well. The cells aggregate and form ECM within a few hours, the magnet is removed, and pipetting is performed to break up the aggregate, once again creating a single cell suspension. Appropriate cell numbers are then transferred to a 384-well assay plate and a ring magnet is positioned below the plate, allowing the cells to be patterned into a new 3D ring shape. Wound healing rates are determined by monitoring ring closure. Two individual fibroblast cell models, HT-1080 fibrosarcoma cells and primary dermal fibroblasts, were tested to compare wound healing rates between cancer cell line and primary cell models. Co-cultures containing fibroblasts and keratinocytes were also examined to ascertain whether more *in vivo*-like cell models have an effect on wound healing rates. Automated kinetic imaging was performed using a novel cell imaging multi-mode reader to track ring closure at regular intervals during the incubation period. The combination provides an easy-to-use, robust method to generate accurate and repeatable results of the effect that new test molecules have on important wound healing applications.

## BioTek Instrumentation

**Cytation™ 5 Cell Imaging Multi-Mode Reader.** Cytation 5 is a modular multi-mode microplate reader combined with automated digital microscopy. Filter- and monochromator-based microplate reading are available, and the microscopy module provides up to 60x magnification in fluorescence, brightfield, color brightfield and phase contrast. With special emphasis on live-cell assays, Cytation 5 features temperature control to 65 °C, CO<sub>2</sub>/O<sub>2</sub> gas control and dual injectors for kinetic assays. Integrated Gen5™ Data Analysis Software controls Cytation 5. The instrument performed kinetic imaging of the 3D cell structure using brightfield and red fluorescent protein (RFP) imaging channels, and a 2x objective.

## Magnetic 3D Levitation and Bioprinting

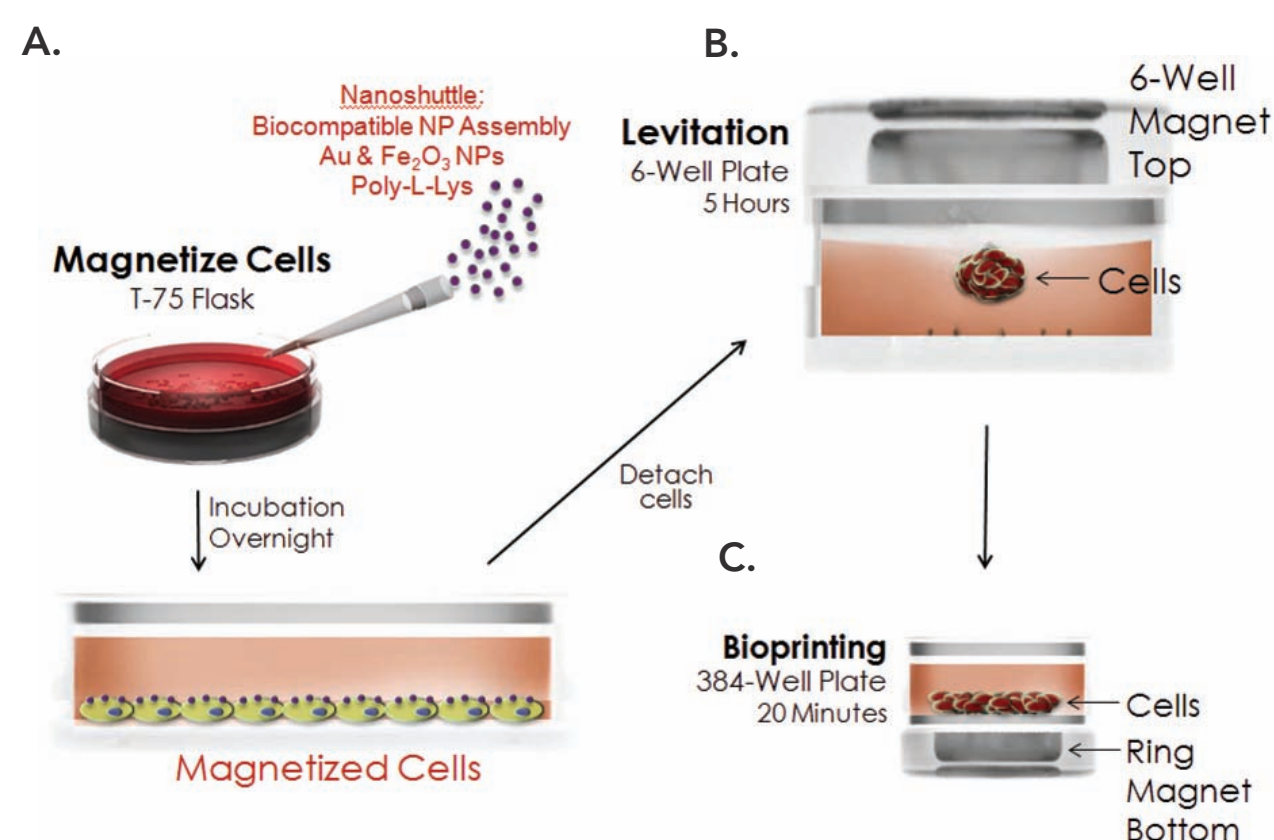


Figure 1. Bio Assay Kit protocol.

The 384-Well Bio Assay™ Kit uses NanoShuttle™-PL, a nanoparticle assembly consisting of gold, iron oxide and poly-L-lysine to (A) magnetize cells. After incubation, (B) cells are detached, resuspended in a cell-repellent plate, and magnetically levitated to aggregate and induce ECM. After breaking up the aggregates, (C) single cells are transferred to a 384-well cell-repellent plate placed atop a 384-well magnetic ring magnet, where they aggregate at the well bottom in the shape of the magnet. Cell rings will contract over time corresponding to wound healing rate of the cell model and well treatment.

## Materials and Methods

**Assay and Experimental Components:** The 384-Well Bio Assay Kit (GBO Catalog No. 781846, consisting of 2 vials NanoShuttle-PL, 6-Well Levitating Magnet Drive, 384-Well Spheroid and Holding Magnet Drives (2), 96-Well Deep Well Mixing Plate, 6-Well and 384-Well Clear Cell Repellent Surface Microplates), prototype 384 well Ring Drive, and additional Cell Repellent Surface 6-Well (GBO Catalog No. 657860) and 384-Well Black µClear® Microplates (GBO Catalog No. 781976), were generously donated by Nano3D Biosciences, Inc. (Houston, TX) and Greiner Bio-One, Inc., (Monroe, NC).

The known inhibitor Cytochalasin D (Catalog No. 1233) was purchased from R&D Systems (Minneapolis, MN).

**Cells:** HT-1080 fibrosarcoma cells (Catalog No. CCL-121) and immortalized keratinocytes (Catalog No. CRL-2309) were obtained from ATCC (Manassas, VA). RFP expressing human neonatal dermal fibroblasts (Catalog No. cAP-0008RFP) were obtained from Angio-Proteomie (Boston, MA).

**Assay Procedure:** T-75 flasks of cell cultures or co-cultures were cultured to 80% confluence, then treated with 600 µL NanoShuttle-PL overnight at 37 °C/5% CO<sub>2</sub>. After incubation, cells were trypsinized, washed, and incubated for 3-5 minutes at 37 °C/5% CO<sub>2</sub>. Cells were removed from the flasks and added to the 6-well cell repellent plate at a concentration of 1.2x10<sup>5</sup> cells/well. A 6-well magnet was placed atop the well plate to levitate the cells, where they aggregated into 3D structures and induced ECM formation during a five hour incubation at 37 °C/5% CO<sub>2</sub>. After incubation, the cells and ECM were broken up, resuspended and added to 384-well cell repellent plate wells at a total concentration of 1.0x10<sup>5</sup> cells/well, in a volume of 37.5 µL, along with 12.5 µL of 4x cytochalasin D, for a final 1x concentration of 10.0 µM. For tests involving co-cultured fibroblasts and keratinocytes, 5.0x10<sup>4</sup> cells from each cell type were added to the well to create the 1.0x10<sup>5</sup> total cell number. A 384-well ring magnet was placed below the well plate, and the assembly was incubated at 37 °C/5% CO<sub>2</sub> for 20 minutes to allow cells to aggregate into the magnet's ring shape. Automated brightfield imaging, using a 2x objective, captured ring closure on all wells every 30 minutes for 16 hours. Automated fluorescence imaging, using the RFP channel, was also performed on wells containing primary fibroblasts as they constitutively express RFP.

## Label-Free Image-Based 3D Wound Healing Monitoring

Following the assay protocol, 100,000 total HT-1080 cells/well, were added to the 384-well cell repellent plate where kinetic brightfield imaging was performed. As illustrated by the lack of ring structure change over time (Figures 2A-B), cytochalasin D inhibits HT-1080 wound healing. Conversely, Figures 3A-D illustrate that the HT-1080 cellular ring contracts in an uninhibited setting, as seen during *in vitro* wound healing, and also demonstrates Cytation 5's ability to track uninhibited cellular ring movement throughout the entire incubation.

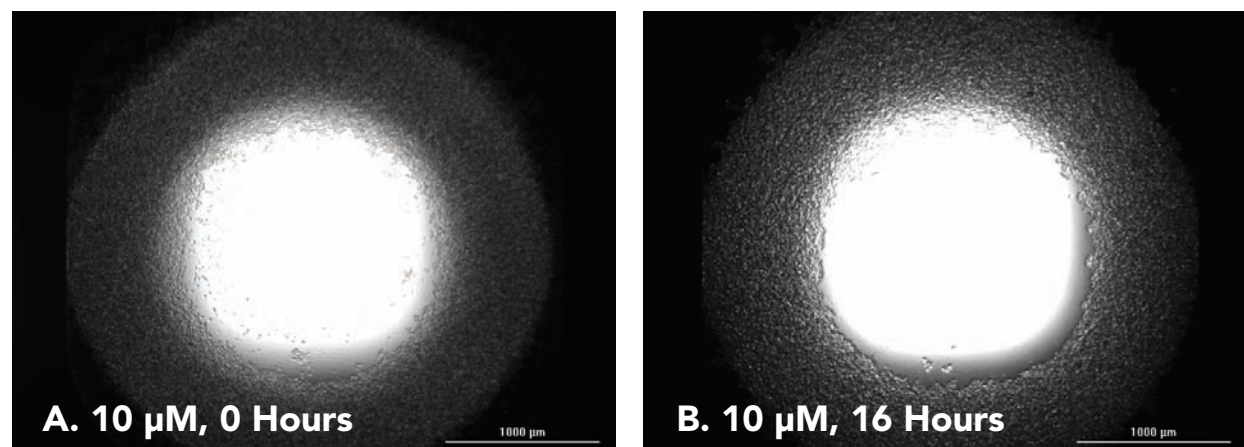


Figure 2. HT-1080 cells treated with cytochalasin D. 2x brightfield images captured from individual wells of HT-1080 cells treated and incubated as follows: (A) 10 µM cytochalasin D, 0 hours incubation; (B) 10 µM cytochalasin D, 16 hours incubation.

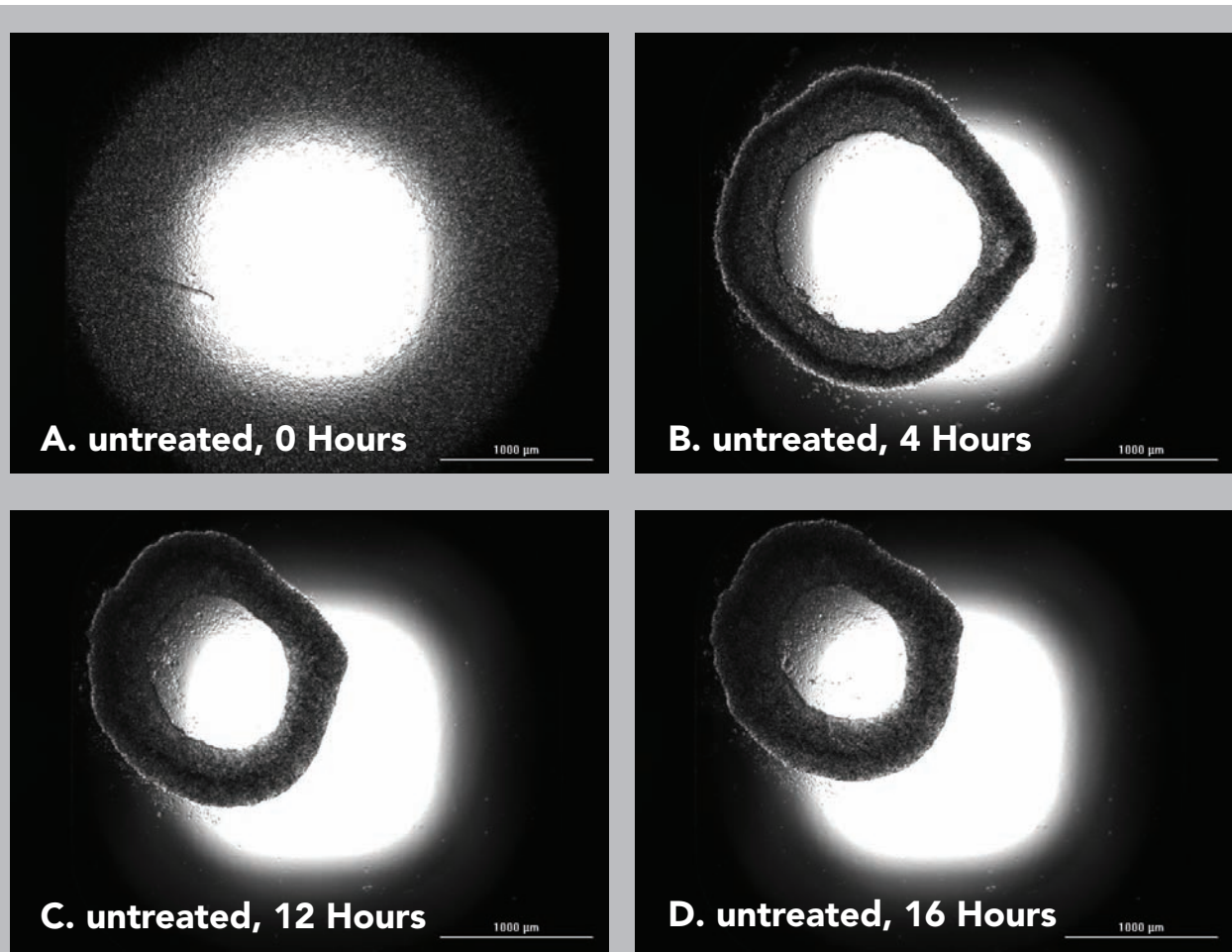


Figure 3. Untreated (0 µM cytochalasin D) HT-1080 cells. 2x brightfield images captured from individual wells of untreated HT-1080 cells incubated for (A) 0 hours; (B) 4 hours; (C) 12 hours; (D) 16 hours.

Next, wound healing extent was analyzed using Cytation 5's brightfield imaging. Object masks were automatically placed around 3D cellular structures (Figure 4) to track parameters such as object size, area and total brightfield signal over the total incubation time. Object area was used for all analyses.

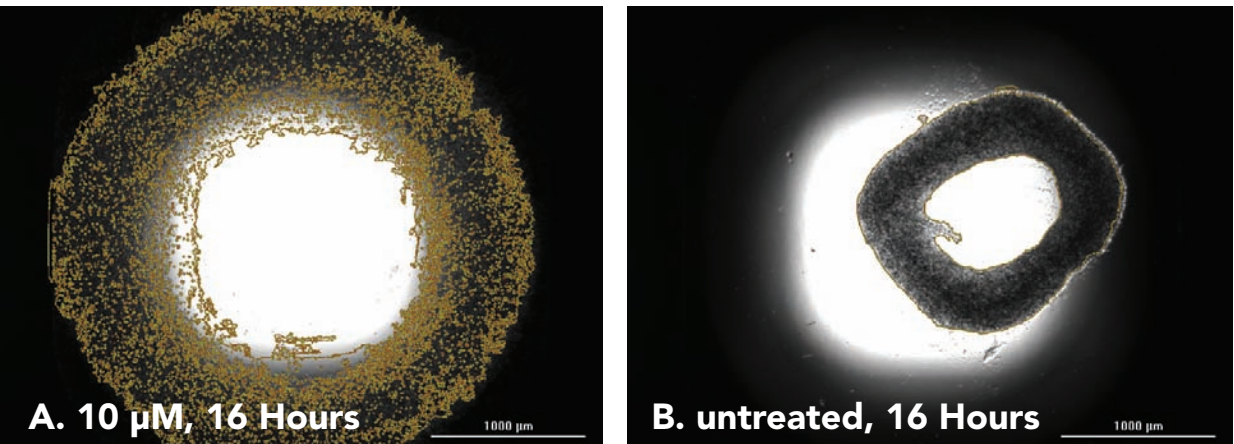


Figure 4. HT-1080 cellular analysis using Cytation 5 2x brightfield imaging. Object masks shown on cells treated and incubated as: (A) 10 µM cytochalasin D, 16 hour incubation; (B) 0 µM cytochalasin D (untreated), 16 hour incubation.

Finally, Cytation 5 calculated the HT-1080 3D cell ring structure's total area for each 30-minute time point, for real-time wound healing analysis. The percent of initial area decreases with time as lower cytochalasin D concentrations are added to the well. Data normalization was carried out by comparing total area at each time point to initial area (Figure 5). Additionally, per Figure 6, Cytation 5 can be used to calculate cytochalasin D IC<sub>50</sub> values using single time point data.

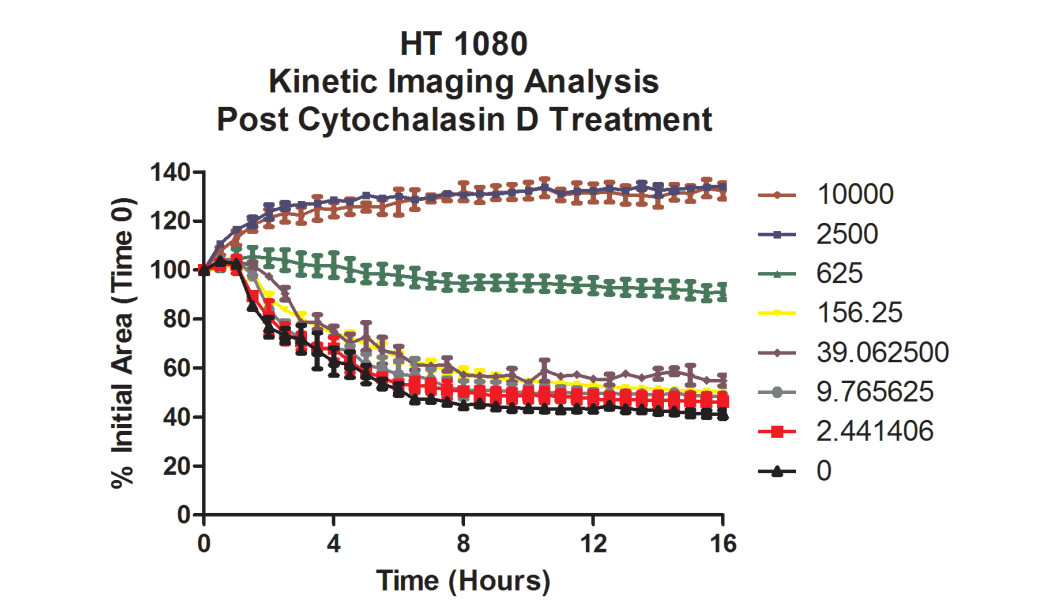


Figure 5. HT-1080 wound healing analysis using dose-dependent percent of initial area. Values represent nM Cytochalasin D concentrations tested per well.

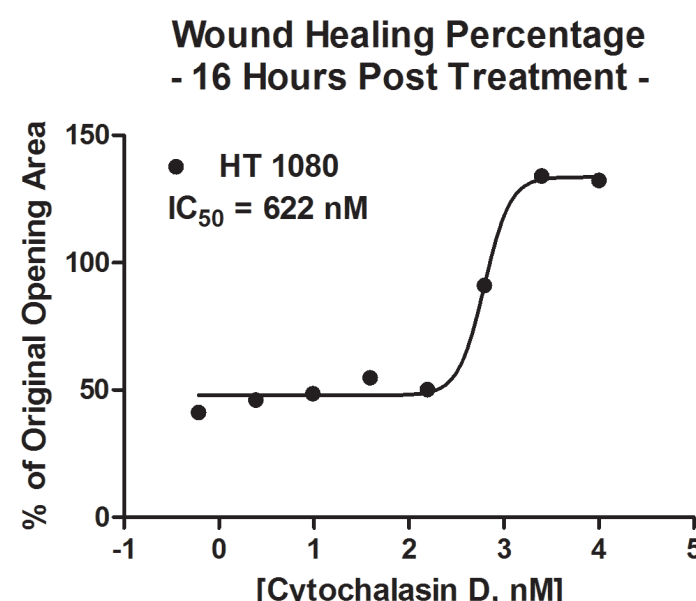


Figure 6. HT-1080 post incubation wound healing IC<sub>50</sub> calculation.

## Primary Fibroblast Comparison

Using immortalized cancer cell lines as surrogate models for primary cells affords the advantage of providing a continuous cell source for experimental purposes. However, internal changes in the cancer cell may modify the migratory characteristics of the cell model as seen by Varani, *et al.* when comparing normal mouse embryo fibroblasts and mouse fibrosarcoma cells. Here we tested human dermal fibroblasts using conditions previously described to examine potential differences primary cells and the HT-1080 fibrosarcoma cell line.

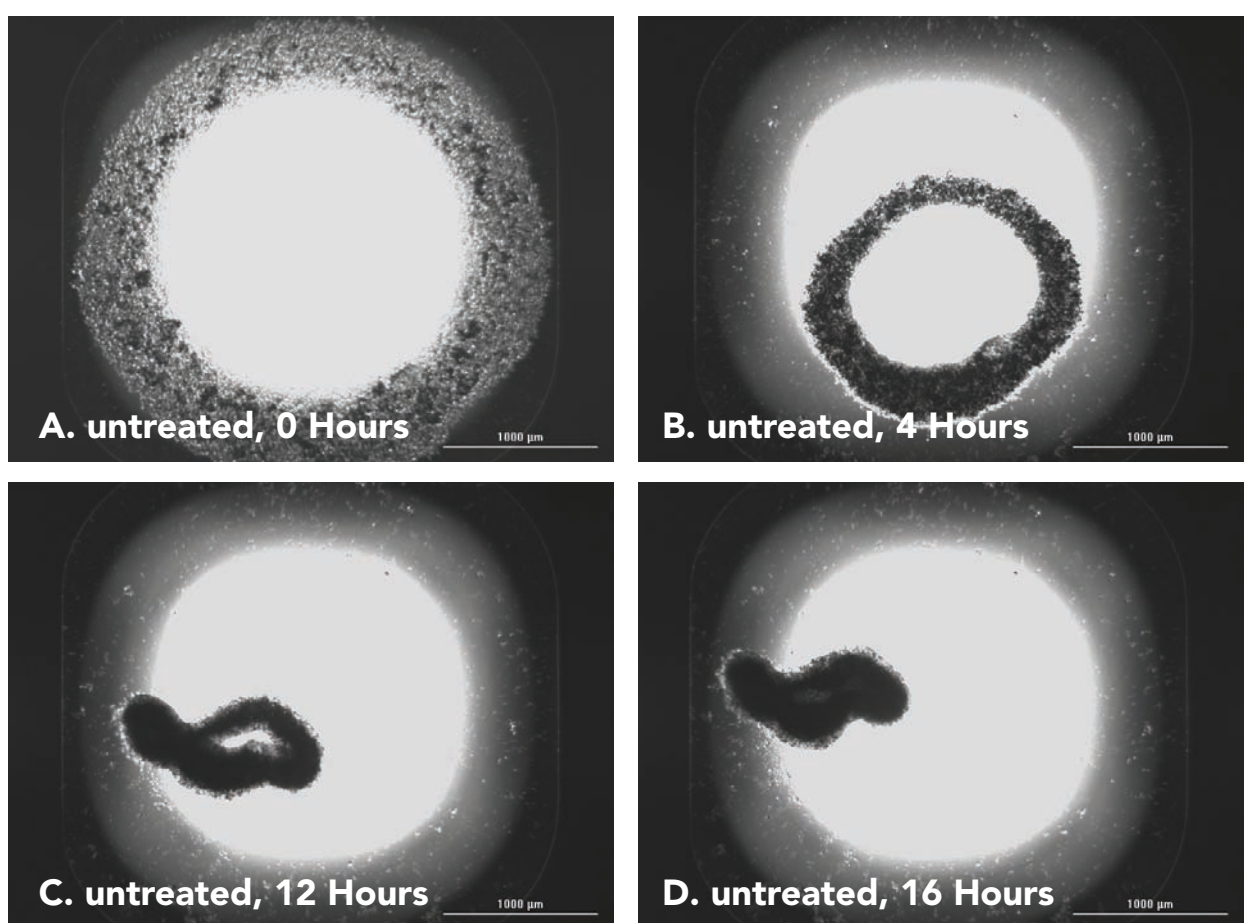


Figure 7. Untreated (0µM cytochalasin D) primary fibroblast cells. 2x fluorescent brightfield images captured from individual wells of untreated primary fibroblast cells incubated for (A) 0 hours; (B) 4 hours; (C) 12 hours; (D) 16 hours.

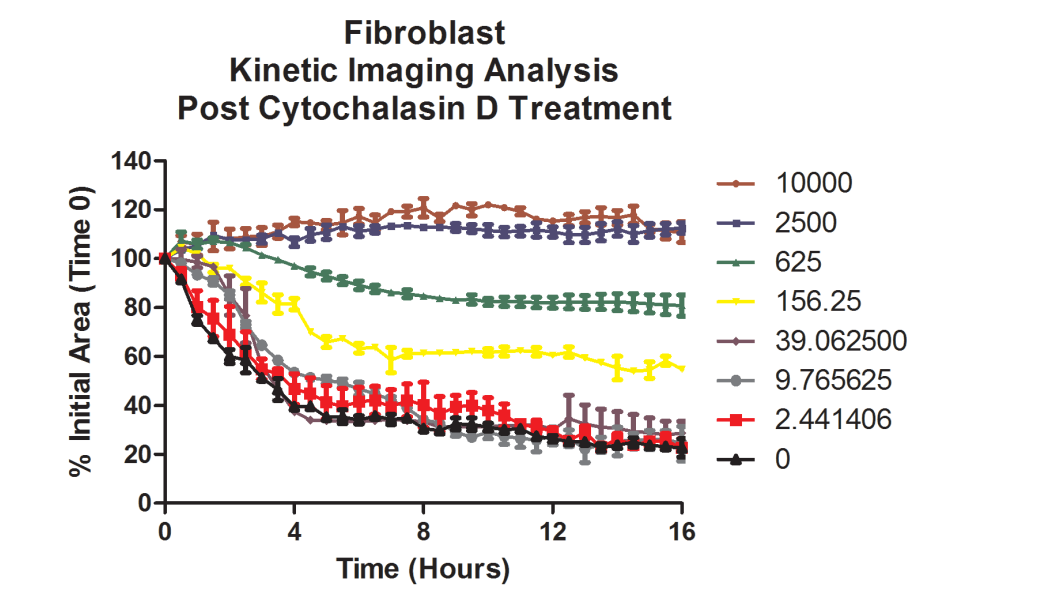


Figure 8. Kinetic primary fibroblast wound healing analysis using dose-dependent percent of initial area.

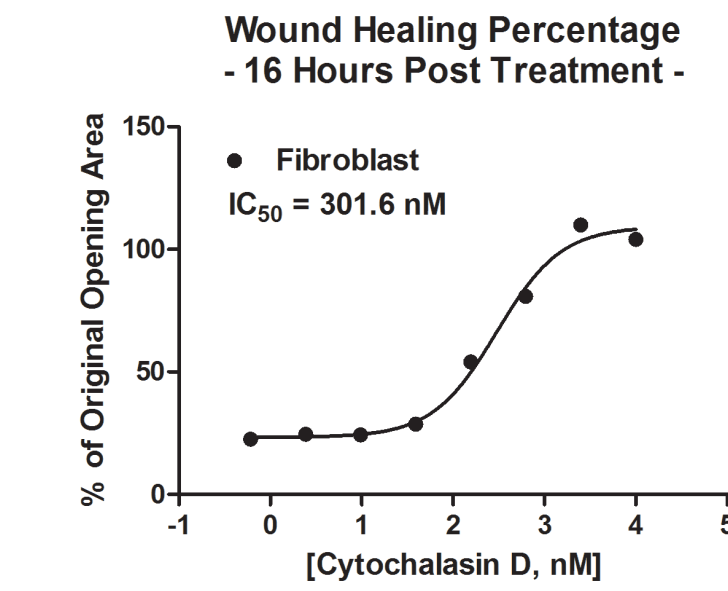


Figure 9. Primary fibroblast wound healing IC<sub>50</sub> calculation.

Cytation 5 was again used to calculate the 3D cell ring total area, created using primary fibroblasts, for wells at each 30-minute time point. A greater percentage of wound healing was seen using primary cells compared to the cancer cell line. Cytochalasin D IC<sub>50</sub> values, using the primary fibroblasts, were calculated (Figure 9) and demonstrated a left shift when compared to values generated with the cancer cell line.

## Primary Fibroblast Comparison (cont.)

Wound healing analysis can also be performed using Cytation 5's fluorescent imaging channels for cells labeled with a fluorescent probe or that constitutively express a fluorescent protein, such as the RFP expressing primary fibroblasts used here. Automated object masks were again utilized to track changes in the 3D cell ring area (Figure 10).

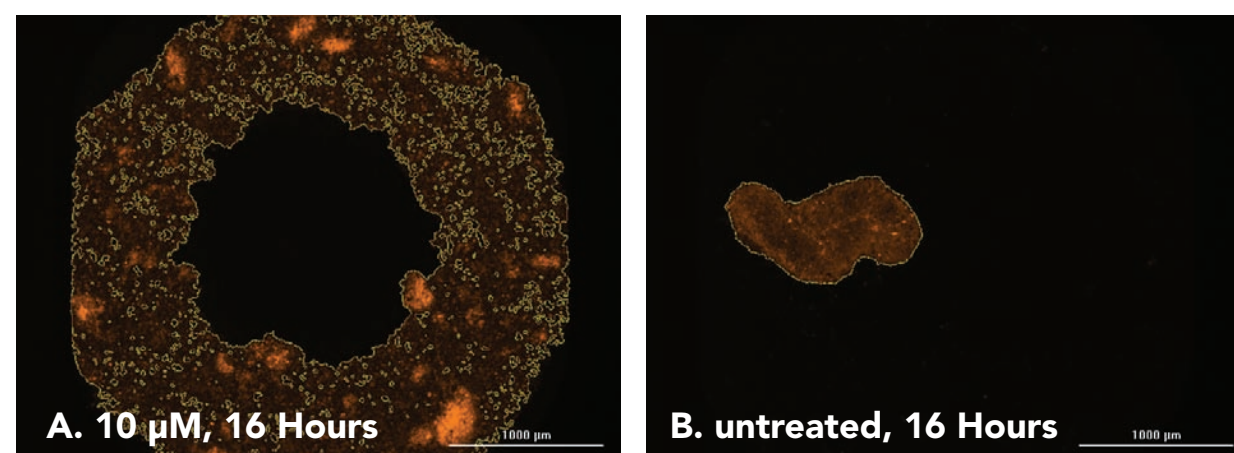


Figure 10. Primary fibroblast cellular analysis using Cytation 5 2x RFP imaging. Object masks shown on cells treated and incubated as: (A) 10 µM cytochalasin, 16 hour incubation; (B) 0 µM cytochalasin (untreated), 16 hour incubation.

When comparing kinetic wound healing patterns (Figure 11) and cytochalasin D IC<sub>50</sub> values (Figure 12) from brightfield and RFP signals, equivalencies were seen.

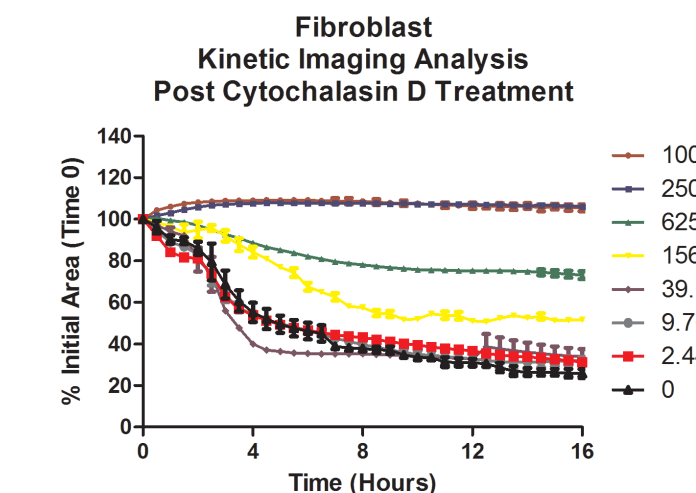


Figure 11. Kinetic primary fibroblast wound healing using RFP channel cellular analysis per cytochalasin D concentration treatment.

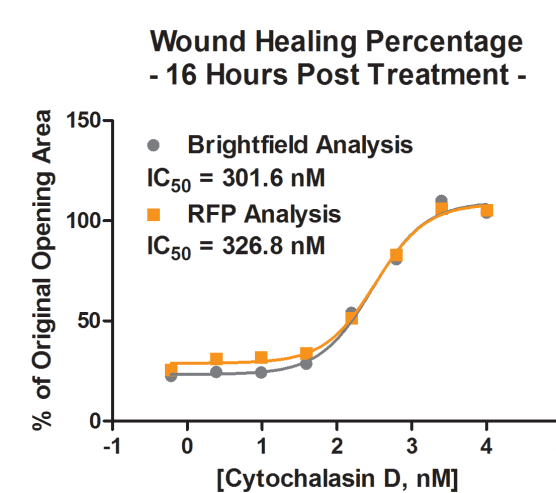


Figure 12. Comparison of primary fibroblast brightfield and RFP IC<sub>50</sub> calculations.

## Fibroblast and Keratinocyte Co-Culture Analysis

Finally, co-cultured wound healing was examined. Werner, *et al.* demonstrated that interactions between keratinocytes and fibroblasts dominate many phases of the wound healing process. Therefore incorporation of a co-culture of these two cell types, as shown below, may provide a more accurate representation of *in vivo* wound healing.

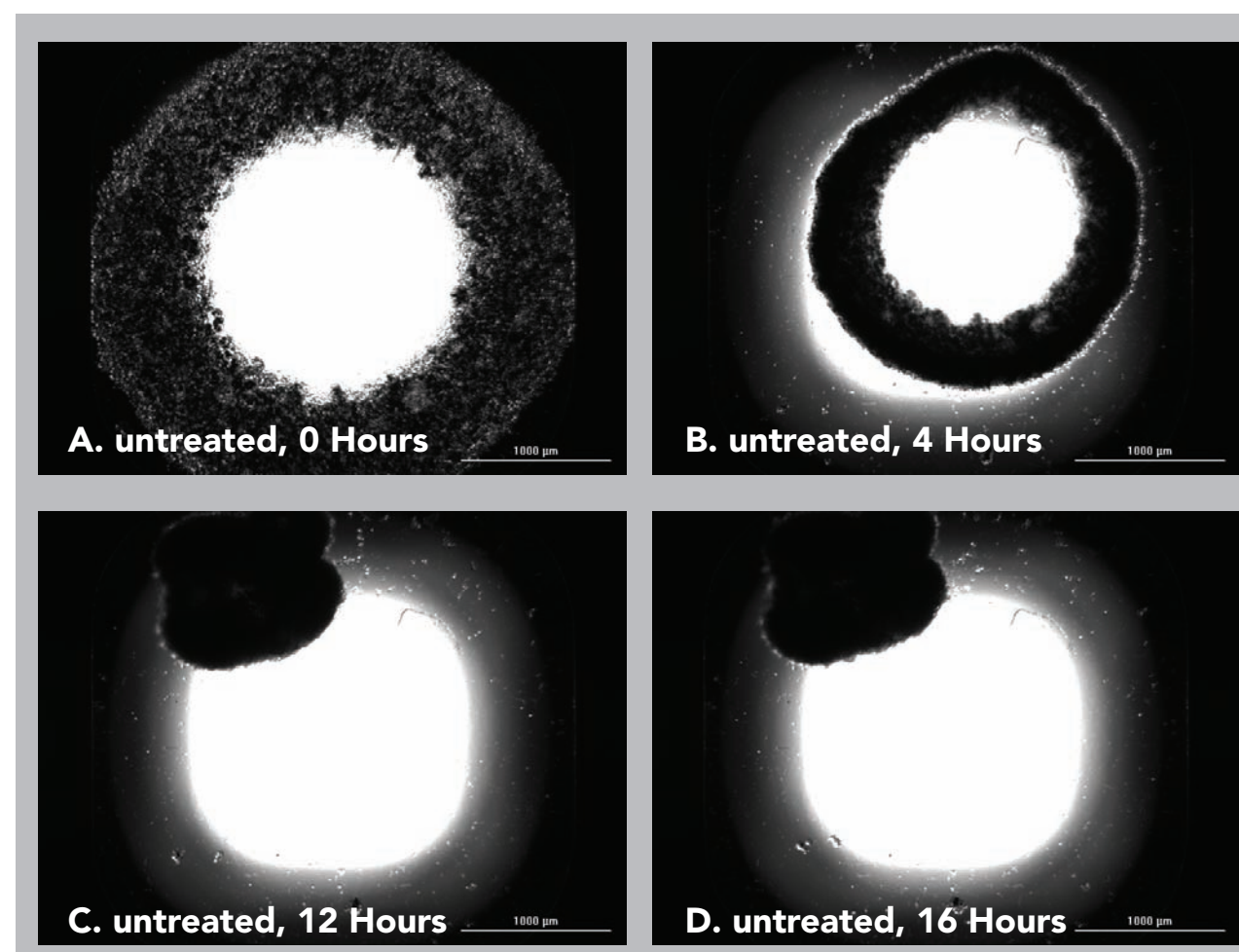


Figure 13. Untreated (0µM cytochalasin) primary fibroblasts and keratinocytes. 2x brightfield images captured from individual wells of untreated co-culture incubated for (A) 0 hours; (B) 4 hours; (C) 12 hours; (D) 16 hours.

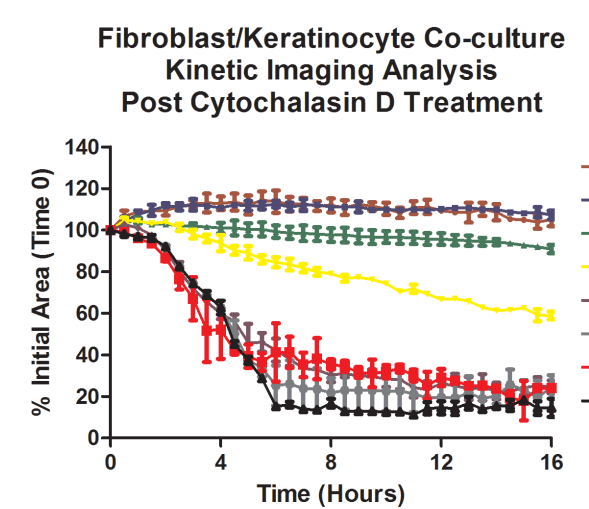


Figure 14. Kinetic co-culture wound healing analysis using cytochalasin D dose-dependent percent of initial area.

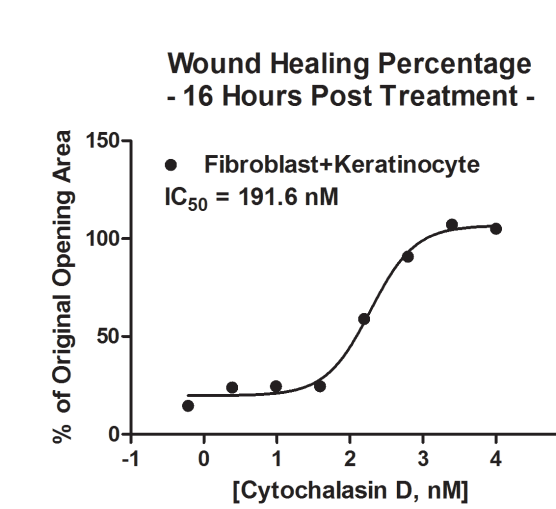


Figure 15. Co-culture post incubation wound healing IC<sub>50</sub> calculation.

Figures 13 and 16, and Figure 17's graph of uninhibited wound healing for all cell models, demonstrate that the fibroblast/keratinocyte co-culture increased wound healing rates compared to fibroblasts alone or cancer cells. The co-cultured 3D ring completely closes by the seventh hour, compared to moderate closure with the remaining cell models. Additionally, the HT-1080 IC<sub>50</sub> curve was distinctly different from the other cell models, as seen in Figure 18. These results validate the need for inclusion of appropriate cell models when performing wound healing analyses.

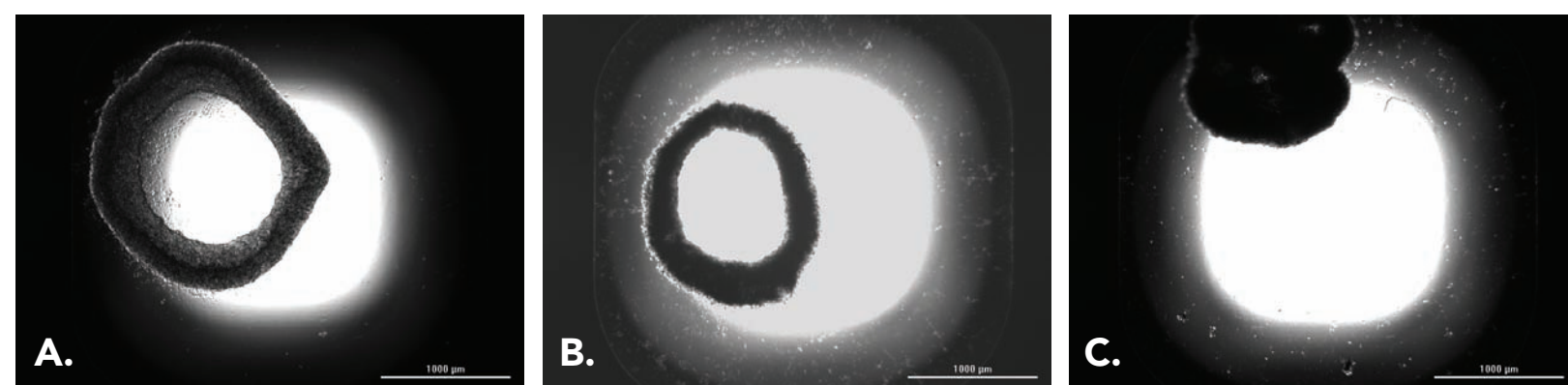


Figure 16. Comparison of cell model wound healing. 2x images captured from untreated (A) HT-1080 cells; (B) primary fibroblasts; (C) co-cultured fibroblasts and keratinocytes; each incubated for 7 hours.

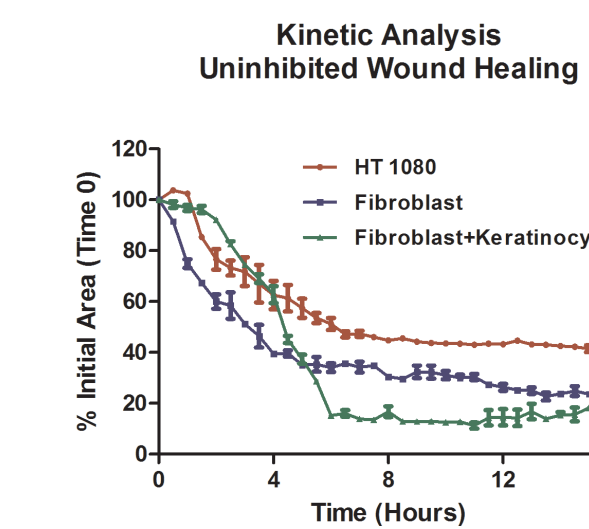


Figure 17. Wound healing rate cell model comparison.

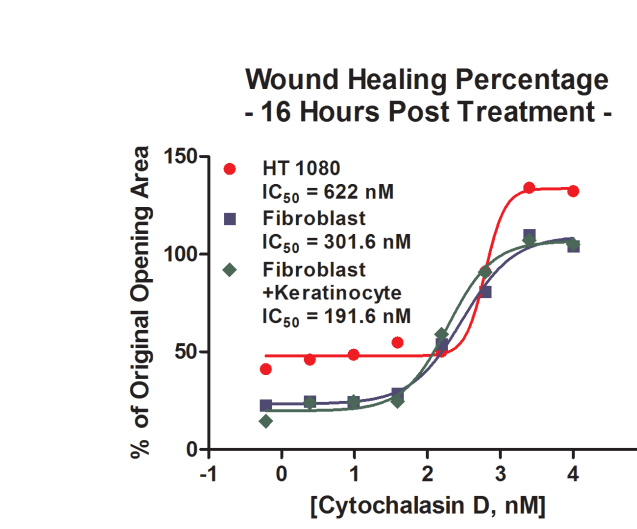


Figure 18. Wound healing IC<sub>50</sub> cell model comparison.

## Conclusions

1. The 384-Well Bio Assay Kit and NanoShuttle-PL particles from nano3D Biosciences provide a simple, robust method to carry out 3D wound healing assessments.
2. Incorporation of Greiner Bio-One Cell-Repellent Surface 6-Well and 384-Well Microplates allow efficient cell levitation for ECM creation, and high throughput performance of the 3D wound healing assay.
3. Cytation's automated imaging and analysis in brightfield and fluorescence imaging channels simplifies the assay process and increases analysis accuracy by removing manual determinations.
4. Use of primary cells may lead to a better understanding of *in vivo* dermal wound healing compared to cancer cells.
5. Use of appropriate cell models, including primary and co-cultured cells, may affect the extent and rate of wound healing, in addition to sensitivity to test molecules.
6. The combination of assay method and automated imaging and analysis creates an easy to use, robust method to generate accurate and repeatable results when used for important dermal wound healing applications.